

# Chitosan biopolymer membranes produced from fishery waste for the adsorption-based removal of lead ions from aqueous systems

Ephraim Igberase\*, Mapula Lucey Moropeng, Mhike Washington

Department of Chemical Engineering, Tshwane University of technology, Pretoria, South Africa

\* Corresponding author E-mail: [ephraimigberase@gmail.com](mailto:ephraimigberase@gmail.com)

## Article info

Received 3/5/2023; received in revised form 26/5/2023; accepted 20/6/2023

DOI: [10.6092/issn.2281-4485/16900](https://doi.org/10.6092/issn.2281-4485/16900)

© 2023 The Authors.

## Abstract

Using a phase inversion technique, chitosan was recovered from the exoskeleton of Cape Rock Lobsters, which are common in the area around Cape Town, South Africa. These flakes were then used to create dense polymer chitosan membranes. Chitosan membrane (CSM) and cross-linked chitosan membrane (XCSM) were characterized by FTIR, XRD, SEM-EDX, and TGA after the chitosan membrane was cross-linked with 2.0% glutaraldehyde. The maximum binding capacity for the developed adsorbent (XCSM) was found to be 2.98 mmol.g<sup>-1</sup> at temperature of 313 K. Equilibrium tests showed that the Langmuir equilibrium model could be utilized to successfully characterize lead binding onto XCSM. The adsorption process was discovered to be endothermic, with an adsorption enthalpy of 52 kJ/mol. As the flux through XCSM increases, the degree of adsorption decreases (1.96-1.36 mmol/g) due to a kinetic process. Co-ions were also found to have an impact on the adsorption of metal ions by XCSM, with the presence of nitrates being found to limit the adsorption and sulphates being found to enhance the adsorption. Using sulphuric acid and hydrochloric acid solutions as eluants, the adsorbed lead ions were recovered. It was discovered that the first was a more efficient eluent. Consequently, a sulphuric acid solution with a pH of 3 might be used to recover up to 95% of the adsorbed lead. But after regeneration, it was discovered that the adsorption capacity had been diminished. This decrease in adsorption capability may be attributed to the membrane losing up to 26% of its bulk during regeneration. After two regeneration cycles, the membrane's structural integrity had been compromised, rendering it useless.

## Keywords

*cross-linked Chitosan membrane; Lead binding; breakthrough curves; binding capacity; metal desorption*

## Introduction

Aquatic organisms' polysaccharide biopolymers are potentially economical and environmentally safe solid adsorbents with a high selectivity for metal ions. Chitosan-metal complexes are created when chitosan biopolymers interact with metal ions in various investigations, usually with the intention of eliminating heavy metals from contaminated water (Igbe-

berase and Osifo, 2019a; Pal and Pal, 2019; Qasem et al., 2021). In particular, studies on chitosan have shown that it has a strong affinity for the metallic ions of aluminum (Cervera et al., 2003), cadmium (Pal and Pal, 2019), chromium (Rojas et al., 2005), copper (Osifo et al. 2017), iron (Ngah et al., 2005), mercury (Finster et al., 2015), lead (Ge et al., 2016; Qu et al., 2021). Chitin, the second most prevalent

polysaccharide found naturally after cellulose, is used to make chitosan. Chitin is a substance found in the exoskeletons of arthropods, crustaceans, and insects that is composed amino sugars with a consistent distribution of acetyl groups. Chitin can be extracted from fungi and algae, but it is exclusively produced commercially from the shell waste of crustaceans, such as crabs, lobsters, prawns, and shrimp. Chitin deacetylation is the process by which chitin is treated in a hot concentration of a strong basic solution, such as sodium hydroxide and potassium hydroxide, to generate chitosan (Singh et al., 2020). The ability of chitosan materials to be converted into flakes or gel that can be molded into different configurations for use in a variety of end-user applications is what makes them useful. It has been widely reported that chitosan gel beads are used in water treatment applications (Guibal, 2004; Milot et al., 1998; Mo et al., 2019; Mokhtar et al., 2023), but research on gel-type membranes is less common. This may be because there is insufficient knowledge about the formulation and uses of these membranes. The production method affects the effectiveness of chitosan membranes for water treatment in terms of flux and adsorption capacity. In earlier research, the transport characteristics of chitosan membranes with regard to metal-ion removal from aqueous solution were examined (Osifo et al., 2017). This study focused on Pb(II) adsorption and looked into the adsorption properties of cross-linked chitosan membranes. To get more knowledge about the suitability of chitosan gel-type biopolymer membranes for water treatment procedures, both the adsorption equilibrium and the kinetics of adsorption and desorption were investigated.

## **Materials and methods**

### **Materials**

Sigma-Aldrich was used to obtain sodium hydroxide (99%), acetic acid (99%), and hydrochloric acid (99%). A pH meter (Hanna HI 8421) was used to change the pH of the solution, and it was bought from Sigma-Aldrich. In the school laboratory, distilled water was created using an Ultima 888 water distiller. The batch adsorption experiment used a shaker (labcon incubator). Acetic acid (99%), hydrochloric acid (99%), and sodium hydroxide (99%) were all purchased from Sigma-Aldrich. The solution's pH was adjusted using a pH meter (Hanna HI 8421), which was purchased from Sigma-Aldrich.

An Ultima 888 water distiller was used to produce distilled water at the school lab. A shaker was utilized in the batch adsorption experiment (labcon incubator).

### **Membrane preparation**

Phase inversion technique was used to create the membranes (Osifo et al., 2017). Other researchers have used this technique to make chitosan beads, including (Guibal, 2004). The chitosan flakes were dissolved in an acetic acid solution to create chitosan solutions with a concentration of 7 wt%. On a level surface, the viscous chitosan solution was poured into a mould (glass plate). For 15 minutes at a constant temperature of 25 °C, the mould and chitosan solution were carefully submerged in a 5-weight percent aqueous solution of sodium hydroxide (97% pure, provided by Saarchem Ltd.). After the membranes were created, they were rinsed in flowing deionized water before being taken off the glass plate together with the moulds. After being taken out of the moulds, the membranes were submerged in deionized water for an hour. The membranes were submerged in deionized water and then washed once more until a pH of zero was reached using new deionized water. The disk-shaped membranes had a diameter of 47 mm and an average thickness of 0.8 (0.02) mm. Only the concentration of chitosan was found to have a significant impact on the solution's viscosity; variations in the concentrations of acetic acid and sodium hydroxide were found not to have an impact.

To stop the membranes from dissolving in acidic media, the membranes were then cross-linked in a 2.0 weight percent solution of glutaraldehyde at 25 °C. Per gram of moist membrane, 1.5 cm<sup>3</sup> of glutaraldehyde solution was employed. The membranes were properly cleaned to get rid of any remaining glutaraldehyde after crosslinking. The physical characteristics of the membranes were identified, classifying them as dense polymer membranes. The membranes had a wet density of 1100 kg.m<sup>-3</sup>, a chitosan content of 5.2 weight percent, a free water volume of 65 weight percent, a fixed water content of 30 weight percent, a maximum pore radius of 40 nm, and a total surface area of 1.15 m<sup>2</sup>. kg<sup>-1</sup>.

The method outlined by (Igberase & Osifo, 2015) was used to calculate the point of zero charge (pH<sub>pzc</sub>) of CSM and XCSM. In a series of flasks, 45

mL of  $\text{KNO}_3$  solution with a known concentration was added. By adding either 0.1 M HCl or NaOH, the solution's initial pH values ( $\text{pH}_i$ ) were controlled from pH 2 to 8. The  $\text{KNO}_3$  solution was added until each flask's total volume of solution reached 50 mL. After noting the  $\text{pH}_i$  of the solution, 0.45 g of adsorbent were added to each flask. The suspensions were periodically manually shaking for 48 hours while they were allowed to equilibrate. The supernatant liquids' ultimate pH values ( $\text{pH}_f$ ) were recorded. The  $\text{pH}_i$  was plotted against the difference between the initial and final pH values ( $\text{pH} = \text{pH}_f - \text{pH}_i$ ). The  $\text{pH}_{\text{PZC}}$  was produced at the intersection of the resulting curve and the point where  $\text{pH} = 0$ .

### Characterization of the membranes

A combined weight of 2.0 g of CSM and XCSM were dried in an oven at 90 °C. The dried membranes were combined to create a powdered form, and then Shimadzu FTIR model 8300 Kyoto, Japan, was used to analyse infrared emissions. The resulting spectra were in the 500–4500  $\text{cm}^{-1}$  range. Using a Shimadzu XRD model 7000, the crystallinity of the membranes was investigated, and intensities between 10 and 90 degrees were recorded ( $2\theta$ ). Using a Shimadzu TGA 8000 Japan, the weight loss of the membranes at various temperatures was investigated. The membranes were coated with gold prior to the SEM analysis, and the morphology of the coated membranes was examined using a Jeol 733 super probe. The device is used in conjunction with an EDX analyser.

### Adsorption and permeation experiments on XCSM

Using analytical grade  $\text{PbSO}_4$  (99% pure supplied by Merck) dissolved in deionized water, a  $\text{Pb(II)}$ -solution with different concentrations of 0.5–1.2  $\text{mmol.L}^{-1}$   $\text{Pb(II)}$  was generated to study the adsorption capacity of XCSM at 20–45 °C. The amount generally reported to be present in the industrial effluent that needs to be treated is this concentration (Dong et al., 2016). To guarantee that the adsorption sites were fully occupied, this relatively high concentration was utilized. The adsorption and flux through the membrane were measured for solutions with varying  $\text{Pb(II)}$  concentrations, that was also made by combining deionized water with analytical grade lead. As previously described (Igberase et al., 2019), a dead-end membrane permeation setup was employed.

To avoid concentration polarization during the permeation tests, the solution was agitated using an overhead stirrer positioned above the membrane. The membrane module was made of a sintered stainless-steel support with an average mesh size of 0.1 mm. Since the support's pore size was at least three orders of magnitude bigger than that of the chitosan membrane, it had almost no movement barrier. While the temperature was regulated using a hot plate (Hydolph MR2002) at various temperatures of 20°C, 25°C, 30°C, 35°C, and 45°C, the membrane was clamped in the membrane holder and the zinc solution could permeate through the membranes under variable feed pressures. The membrane holder was filled with the  $\text{Pb(II)}$  solutions, and the temperature was watched until it remained steady. Then, under a transmembrane pressure of 50 kPa, the adsorption and permeability (or flux) were determined. Pressurized nitrogen was used to apply the pressure differential to the cell. One liter (1 L) of each of the different  $\text{Pb(II)}$  solutions was passed through the membranes until the permeate's  $\text{Pb(II)}$  concentration reached steady-state, or until the  $\text{Pb(II)}$  concentration remained constant, in order to ensure observations of the steady-state transport parameters. The adsorption experiment was carried out in triplicates. The permeate  $\text{Pb(II)}$  concentrations were measured quantitatively using an Atomic Absorption Spectrophotometric Analyzer with a Perkin Elmer, Analyst 200 Model B3150070 at predetermined time intervals. According to Eq, the flux is defined as the volume that passes through the membrane per unit of time and area, as shown in Eq. 1.

$$J_v = \frac{V}{A \cdot t} \quad [1]$$

where  $V$  is the volume of liquid permeating through the membrane in  $\text{m}^3$ ,  $A$  is the membrane surface area in  $\text{m}^2$ , and  $t$  is the duration in seconds.  $J_v$  is the flux through the membrane in  $\text{L.m}^2/\text{hr}^{-1}$ .

while the amount of heavy metals absorbed per unit dry adsorbent is used to characterize the adsorption capacity (Farooq et al., 2010):

$$q_e = \frac{(C_{in} - C_e) \cdot V}{m} \quad [2]$$

where  $C_{in}$  and  $C_e$  are the initial and final concentrations of  $\text{Pb(II)}$  in the solution, respectively, in  $\text{mmol/L}$

and  $q_e$  is the equilibrium adsorption capacity in mmol/g chitosan. The speciation of the Lead-ions and the tendency for precipitation, both with regard to solution pH, required to be established in order to guarantee reliable results from the adsorption and permeation studies. A similar method to Guibal's was used to compute the speciation of Lead with regard to pH using the OLI program (Guibal 2004). More than 99.8% of the Lead-ions were discovered to be in the  $Pb^{2+}$  configuration under the experimental circumstances of this study (pH 6), whereas the creation of other species (such as  $Pb(OH)$ ) was found to be minimal. By examining how the pH of the solution affected the precipitation of Lead hydroxide  $Pb(OH)_2$  at various  $Pb(II)$  concentrations, it was also possible to identify the limits of Lead hydroxide precipitation (0.612-7.65 mmol.L<sup>-1</sup>). At these ranges of  $Pb(II)$  concentrations, it was discovered that a drop in  $Pb(II)$  concentration happened at a pH value >6. Therefore, the precipitation of  $Pb(II)$  hydroxide from solution might be attributed to the drop in  $Pb(II)$  concentration above a pH of 6. The drop in  $Pb(II)$ -ion concentration will instead be caused by a mix of adsorption by the chitosan membranes and precipitation if the adsorption trials aren't carried out at a pH of 6 or below for high  $Pb(II)$  concentrations. Consequently, in this investigation, a Jenway 3310 pH meter, diluted sulphuric acid (98% pure supplied by Saarchem Ltd), diluted sodium hydroxide (97% pure supplied by Saarchem Ltd), and other chemicals were used to maintain.

the pH of the  $Pb(II)$  input solution at a pH of 5-6

## Results and discussion

### Characterization result

**FTIR result.** To identify the fundamental functional groups and check if glutaraldehyde was successfully attached to the chitosan membrane, the FTIR spectrum was used. The plot of Figure 1 is explained by the absorption band at wavelengths 3357  $cm^{-1}$  and 3322  $cm^{-1}$  for CSM and XCSM, respectively, which indicates the existence of exchangeable protons from the alcohol and amine group (Ayub & Raza, 2021; Ge et al., 2016; Ge & Hua, 2016; Sheth et al., 2021). Protons that can be exchanged during the chemical cross-linking process may be the cause of the minor shift in the band. The deformation of  $CH_2$  and  $CH_3$  is indicated by the alkenyl C-H stretch at wavelengths of 2921  $cm^{-1}$  and 2922  $cm^{-1}$  for CSM and XCSM, respectively. The steep peaks for CSM and XCSM respectively, at 1561  $cm^{-1}$  and 1602  $cm^{-1}$ , correspond to aromatic C=C bending vibrations. The peak at 1427  $cm^{-1}$  for CS and 1375  $cm^{-1}$  for XCSM represents  $CH_2$  and  $CH_3$  bending vibrations respectively. In CSM and XCSM, a sharp peak of 1000  $cm^{-1}$  was seen, indicating C-O stretching vibration. It is possible to attribute the peak at 879  $cm^{-1}$  for CSM and 774  $cm^{-1}$  for XCSM to C-H bending vibration. Additional peaks at wavelengths of 1211  $cm^{-1}$  and 1272  $cm^{-1}$ , which are attributable to C-N stretching vibration, further support the cross-linking of glutaraldehyde onto CSM.

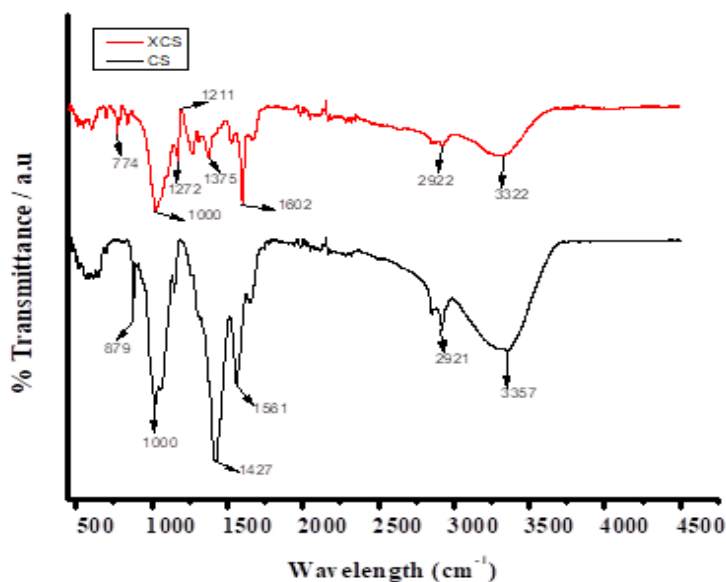


**Figure 1**  
*FTIR of CS and XCS*  
*respectively*

**XRD result.** The diffraction pattern of CSM and XCSM is shown in Figure 2. Since chitosan may be modified while retaining part of its features, both membranes shared a characteristic of 2, which corresponds to 110 planes of chitosan (Igberase &

Osifo, 2019a; Pal & Pal, 2019; Singh et al., 2020). However, in the case of XCSM, the intensity was raised as a result of a chemical cross-linking reaction, which demonstrated that CSM and glutaraldehyde had been chemically connected.

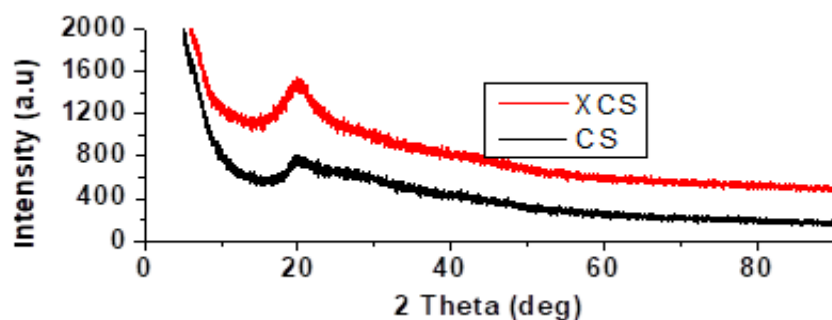


**Figure 2**  
XRD of CSM and XCSM

**TGA result.** TGA was used to determine the thermal characteristics of CSM and XCSM when heat is applied. To investigate the thermal stability of the membranes, a weight versus temperature plot was made. The stages of CSM and XCSM thermal degradation are depicted in Figure 3.

In the first stage, which took place between 40 and 157 °C, there was a 10% weight loss, which is equivalent to the loss of water (Madhava Rao et al., 2006).

The second stage had a weight loss of 38% and ran from 200 °C to 350 °C.

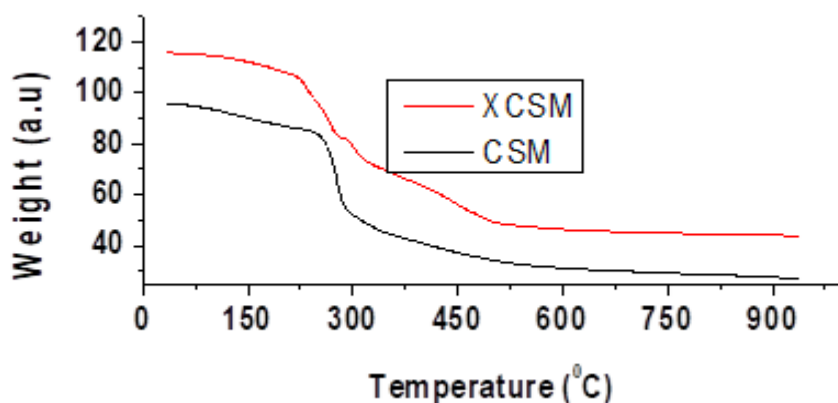


**Figure 3**  
TGA of CSM and XCSM

Dehydration of the saccharide rings, depolymerization, and disintegration of the acetylated and deacetylated units of adsorbent are attributed to this weight loss (Igberase et al., 2019). Over 400 °C, there was a 54% weight loss in the third stage. Chitosan membrane that is not cross-linked is being broken down at this point. During the initial stage of degradation when glutaraldehyde was cross-linked with chitosan membrane, a 5% weight loss was noticed at temperatures between 34 and 141 °C. With a 31% weight loss, the second stage began at 227 °C and went up to 330 °C..

Above 500 °C, there was a 15% weight loss in the third stage. This weight loss in the first, second, and third stages is due to the removal of surface water, depolymerization, and decomposition of the acetylated materials, respectively (Omorie et al. 2016).

**SEM result.** Using a scanning electron microscope, the morphology of CSM and XCSM was studied (SEM). The cross-linking of glutaraldehyde on the surface of the chitosan membrane led to the evenness of the surface, showing that

glutaraldehyde was chemically attached to the surface of the membrane (Madhava Rao et al., 2006; Rao et al., 2008). SEM pictures with a magnification of 50 x alongside EDX data are provided in Figure 4 a and b. The EDX results showed that the membranes contained a number of essential elements. The elements found in CS (N, C, H, and O) were also found in XCSM, with the exception of the percentage weight of N, which decreased after the cross-linking reaction.

This may be expected given that some of the amine group of chitosan is involved in the cross-linking reaction (Jin et al., 2020; Mo et al., 2019; Qasem et al., 2021; Sajjadi et al., 2019). However, it was found that XCSM had more C, O, and H due to glutaraldehyde cross-linking. Figure 4 shows a schematic illustration of the cross-linking procedure. In this figure, glutaraldehyde forms intermolecular bridges across chains and preferentially links with nitrogen.

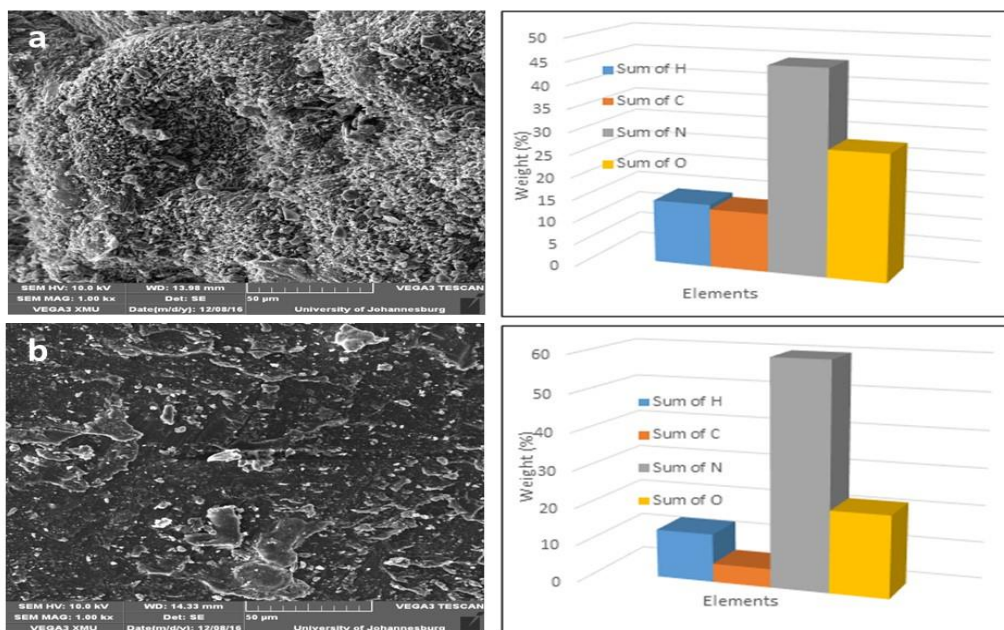


**Figure 4 a,b**  
SEM/EDX of CSM and XCSM respectively

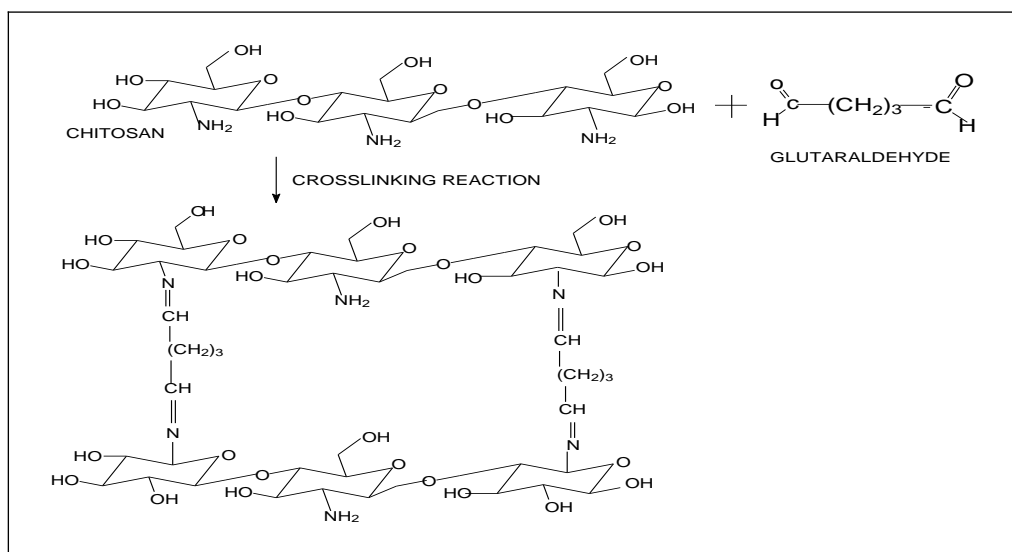


**Figure.5**  
Schematic representation of the cross-linking process of chitosan

### The effect of $\text{pH}_{\text{PZC}}$

The  $\text{pH}_{\text{PZC}}$  of the adsorbent can also be used to describe the influence of pH. The CSM  $\text{pH}_{\text{PZC}}$  was discovered to be 4.41, while the XCS  $\text{pH}_{\text{PZC}}$  was

shown to be 4.87 (Fig. 6). The decrease in acidic groups caused by the reaction of glutaraldehyde with acidic groups generating amide linkages which reduces the total acidity, is what caused the  $\text{pH}_{\text{PZC}}$ .

to rise from 4.41 for CSM to 4.87 for XCSM. The pH at which the total measured charge is zero on the surface of the adsorbent is called  $pH_{PZC}$  (Farooq et al., 2010; Geng et al., 2022; Mao et al., 2021). The protonation of some functional groups occurs when an adsorbent is dissolved in a solution with a pH lower than  $pH_{PZC}$  of the adsorbent, and the adsorbent then behaves like a positively charged poly-matrix. This attracts the negatively charged ions that is present in the solution. The oxyanions of some metals, such arsenate and chromate, which are negatively charged, are the exception to the rule that metal ions are often positively charged. The adsorbent is now drawing these negative ions to it. The functional groups on the adsorbent deprotonate above this pH level, behave as negative species, and bind the positive metal ions as a result. However, the adsorbent's surface is neutral at  $pH = pH_{PZC}$ , positively charged at  $pH < pH_{PZC}$ , and negatively charged at  $pH > pH_{PZC}$ . Given that the surface is negatively charged, the  $pH_{PZC}$  of CSM and XCSM was lower than the pH of the solution, which encouraged adsorption.

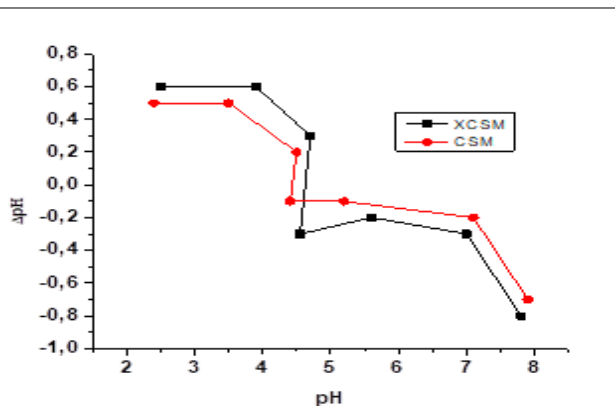


**Figure 6.** Influence of point of zero charge on chitosan membrane and cross-linked chitosan membrane

### Adsorption capacity

Figure 7, displays the outcomes of equilibrium adsorption tests using XCSM and lead ions at a pH of 5 and a range of temperatures (between 293 K and 313 K). It was noted that the permeate's pH was somewhat higher than the feed solution's (an average increase of 0.2 was observed). Because chitosan has a strong affinity for the Pb(II)-cations, the shape of the adsorption isotherms demonstrates a quick initial increase in adsorption capacity.

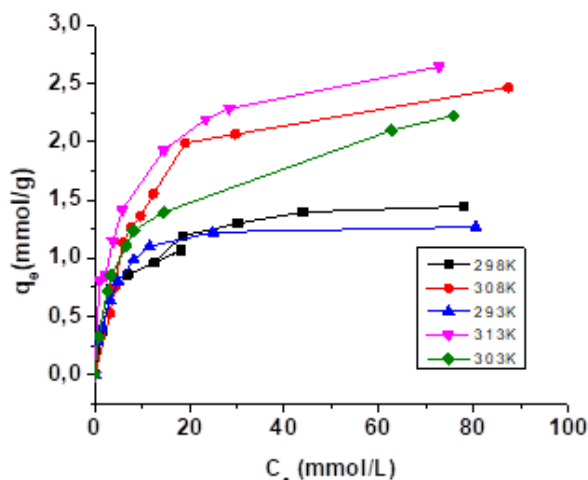


**Figure 7.** Experimentally measured equilibrium adsorption isotherms of Pb(II) onto XCSM at different temperatures and at a pH of 5, the data point represents average value of experiment performed in triplicates

The adsorption of Pb(II) onto the XCSM was modelled using the Langmuir and Freundlich adsorption isotherms. The most used model for describing metal ion adsorption on chitosan is the Langmuir model (Bouhamed et al., 2012; Farooq et al., 2010). The Langmuir model presupposes homogeneous adsorption energies on the surface and a lack of sorbent transmigration in the plane of the surface. For monolayer sorption on a surface with a limited number of sites, this model is applicable, and is represented by Eq. [3]:

$$\frac{C_e}{q_e} = \frac{C_e}{Q_m} + \frac{1}{Q_m b} \quad [3]$$

Equation [3] defines  $C_e$  as the equilibrium concentration of metal ions in mmol.  $Q_e$  and  $Q_m$  are the equilibrium and maximum adsorption capacities, respectively. A measure of the strength of the link between the adsorbate and the adsorbent,  $L^{-1}$ ,  $b$  is the affinity parameter in  $L \cdot mmol^{-1}$ . The affinity parameter  $b$  and the maximal adsorbent capacity,  $Q_m$ , can be calculated using the linear plot of  $C_e/q_e$  versus the equilibrium concentration,  $C_e$ . According to (Bouhamed et al., 2012), the separation factor ( $R_L$ ), which is used to assess whether an adsorption system is favorable or not, can be utilized to represent the fundamental properties of the Langmuir model.

(Madhava Rao et al., 2006), the conditions of  $R_L > 1$ ,  $R_L = 1$ , and  $R_L$  between 0 and 1 indicate unfavorable, linear, and favorable conditions, respectively.

$$R_L = \frac{1}{1 + bC_o} \quad [4]$$

The Freundlich model, which represents a semi-empirical relationship between the adsorbate concentration and the adsorbed concentration, is the second most used isotherm model (Nghah et al. 2005; Wan Nghah et al., 2012). The Freundlich model's linearized form, denoted by Eq. [5], can be used to calculate the adsorption intensity and capacity. The parameter  $n$ 's value falls within the range of 1 to 10 under typical adsorption conditions (Madhava Rao et al., 2006).

$$\log q_e = \log K_F + \frac{1}{n} \log C_e \quad [5]$$

where  $K_F$  and  $n$  (dimensionless constants) stand for, respectively, adsorption capacity and intensity (Madhava Rao et al., 2006).

It was determined that the Langmuir model provided the most accurate description of the data based on the linear fits to the Langmuir model's  $R^2$ -values of 0.98 to 0.99 and the linear fits to the Freundlich model's  $R^2$  values of 0.72-0.84. According to Table 1 calculation of the Langmuir equilibrium constants based on Figure 5, the adsorption capacity rises with temperature, reaching a value of 2.45 mmol.g<sup>-1</sup> at 303 K and higher. The fact that chitosan membranes are gel-type membranes where the free water volume plays a substantial role may help to explain this temperature-related rise (Yu et al., 2021).

Temperature (K)	Langmuir			Freundlich		
	$Q_m$ (mmol Pb.g <sup>-1</sup> chitosan)	$b$ (L.mmol <sup>-1</sup> )	$R^2$	$K_F$	$n$	$R^2$
293	1.32	1.11	0.99	0.65	2.34	0.84
298	1.76	1.45	0.98	0.69	2.21	0.76
303	2.22	1.87	0.98	0.75	2.33	0.72
308	2.98	1.99	0.99	0.97	2.54	0.76
313	2.01	1.01	0.97	0.77	2.10	0.74

**Table 1**

*Langmuir and Freundlich model constants for Pb(II) adsorption onto XCSM at a pH = 5 and at varying temperature.*

According to (Barique et al., 2017), an increase in temperature causes the membrane to stretch, increasing the volume of free water as a result. This could make the adsorption sites easier to access and lead to a higher adsorption capacity. The adsorption capacity, however, stays mostly unchanged at temperatures over 303 K, while this impact is only present below 303 K. For lead adsorption onto XCSM at concentrations of 7.65 mmol/L and temperatures of 293, 298, 303, 308, and 313 K, the  $R_L$  values obtained from Eq. (4) were 0.09, 0.10, 0.09, 0.08, and 0.09, respectively. These results point to favourable isotherms.

The adsorption capacity found in this work is greater than that reported by Becker et al. for chitosan beads (Becker et al., 2000) and Bassi et al. for chitosan flakes (Bassi et al., 2000a).

Adsorption capabilities of less than 1.53 mmol.g<sup>-1</sup> for comparable process conditions were recorded in

both of the aforementioned experiments. Although the pH of the solution was not stated, (Ho & McKay, 2002a) found that chitosan powder had an adsorption capacity of 2.5 mmol.g<sup>-1</sup> and a Langmuir affinity value of 0.46 - 0.85 L.mmol<sup>-1</sup>. Osifo et al., 2017, employed chitosan beads made from the same raw material as in this investigation to determine the maximum adsorption capacity, which was found to be 1.065 mmol.g<sup>-1</sup> at a pH of 5. This comparison of chitosan beads and membranes raises the possibility that membranes might offer an edge in terms of adsorption capacity. In addition to increasing the transport rate, the forced contact between water and chitosan in the membrane (caused by the convective transport of the water through the membrane) may also enhance the contact between the metal ion and the functional groups of chitosan, leading to a greater capacity for adsorption.

The Van't Hoff equation can be used to analyse how

temperature affects the affinity parameter  $b$  in the Langmuir model as seen in Eq. [6]:

$$b = b_o \cdot \exp\left(-\frac{\Delta H_{ads}}{R \cdot T}\right) \quad [6]$$

where  $\Delta H_{ads}$  is the adsorption enthalpy in  $\text{J}\cdot\text{mol}^{-1}$ ,  $b_o$  and  $b$  are the affinity parameters at temperatures  $T_o$  and  $T$ , respectively,  $R$  is the universal gas constant ( $8.3144 \text{ J/mol}\cdot\text{K}$ ), and  $T$  is the temperature in  $\text{K}$ . Therefore, to ascertain the enthalpy of adsorption, the linear form of the Van 't Hoff equation in Eq. [7].

$$\ln(b) = \ln(b_o) - \frac{\Delta H_{ads}}{R \cdot T} \quad [7]$$

Accordingly, the results of the linear regression, revealed that the enthalpy of adsorption of  $\text{Pb(II)}$  onto the cross-lined chitosan membranes was  $52 \text{ kJ}\cdot\text{mol}^{-1}$ . The results shown in Table 1 confirm that the observed adsorption enthalpy points to an endothermic adsorption, which favours the adsorption of  $\text{Pb(II)}$  as temperature rises. For the adsorption enthalpy of  $\text{Pb(II)}$  adsorption on chitosan, (Ho and McKay, 2002; Lima and Airoidi, 2004; Sajjadi et al., 2019; Taty-Costodes et al., 2005) discovered negative values ( $-27.7 \text{ kJ}\cdot\text{mol}^{-1}$  for beads and  $-17.7 \text{ kJ}\cdot\text{mol}^{-1}$  for powder). Exothermic reactions are the norm for adsorption. However, (Ho and McKay 2002) showed favourable adsorption enthalpies for the adsorption of copper and mercury on chitosan powder (Farooq et al., 2010). As was noted with the

rise in adsorption capacity with an increase in temperature, this behavior may also be linked to the effect of temperature on the free water volume of the chitosan. The phenomena of adsorption will depend on the types of interactions (reactions) that are taking place between the solute and the adsorbent when a solute, such as metal ions, are adsorbed on an adsorbent medium, such as chitosan. Most often, the amount of energy involved is used to categorize the type of adsorption, which can either be chemical (i.e., the interaction is a covalent bond between the solute and adsorbent) or physical (the interaction is a van der Waals force) in nature.

The amount of energy required for adsorption in both cases has been reported; for physical adsorption (involving Van der Waals forces), the enthalpy range was found to be  $20\text{--}100 \text{ kJ}\cdot\text{mol}^{-1}$ ; for chemical adsorption (involving covalent bonding), the enthalpy range is  $200\text{--}500 \text{ kJ}\cdot\text{mol}^{-1}$ ; and in both cases, the process is typically exothermic (Igberase & Osifo, 2019b). One of the most important aspects of the adsorption process is the quality of the bond between the adsorbent and the adsorbate (Ho & McKay, 2002a). Adsorbent and adsorbate with a strong bond have greater adsorption capacity, but desorption of the adsorbate from the adsorbent is more challenging. Table 2 compares the capacity of chitosan membranes to other chitosan formulations and other adsorbents (only the maximum values found in literature are given). Cross-linked chitosan membranes have a high adsorption capacity in contrast to other chitosan formulations and other adsorbents, according to this study (Table 2).

Material	binding capacity ( $\text{mmol}\cdot\text{g}^{-1}$ )	Reference
Cross-linked chitosan membranes	2.98	This study
Chitosan powder	2.51	(Ho & McKay, 2002b)
Chitosan flakes	1.27	(Bassi et al., 2000b)
Chitosan beads	1.06	(Igberase et al., 2014b)
Chitin	0.27	(Chui et al., 1996)
Activated sludge	0.38	(Jaafari et al., 2004a)
Lignin	1.45	(Kurita et al., 2003a)
Activated carbon (GAC-C)	0.28	(Kurita et al., 2003b)
Peat moss	0.20	(Kurita et al., 2003b)
Bentonite	0.81	(Kurita et al., 2003b)

**Table 2.**  
*XCSM adsorption compared to other adsorbent binding capacities for  $\text{Pb(II)}$  in literature.*

### The effect of flux on adsorption

The solution was only circulated once through the membrane during these tests, which were carried out under non-steady state circumstances. This was carried out to find out if high flux ratios have an effect on adsorption capacity. As a result, Figure 8 illustrates how flow affects the adsorption of Pb(II) by the chitosan membrane. Since the flow is dependent on the transmembrane pressure, this was changed until a particular flux was obtained, at which point the adsorption was calculated. Figure 8 makes it obvious that as the flow increases, the Pb(II) loading decreases.

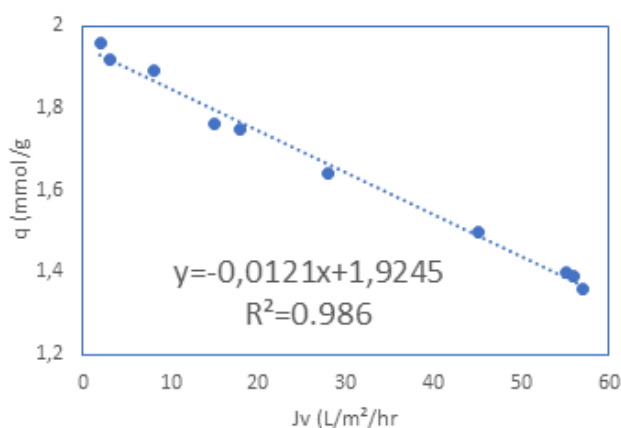


**Figure 8.** The relationship between Pb(II) adsorption and membrane flux (Non-equilibrium, pH = 6, temperature = 298K, and 0.75 mmol.L<sup>-1</sup> Pb(II))

The shorter adsorption time is the reason behind this. As a result, the process is kinetic; the lower the adsorption, the higher the flux. Therefore, it can be said that internal diffusion contributes to the adsorption kinetics. A linear relationship between the adsorbed Pb(II) and the transmembrane flow was obtained based on the observed flux range. It is also important to note that if one extrapolates to 0 flux, the capacity is 1.82 mmol.g<sup>-1</sup>, which equates to the value in Table 3. However, the linear connection also appears to break down as the flux approaches 0, which means that at this point, the capacity is 1.82 mmol.g<sup>-1</sup>.

### Breakthrough studies

One of the most important aspects of designing an adsorption system with metal ions residence time, the reactor, and the reactor controlled by the kinetics of the system is estimating the rate at which binding happens for the given system (Igberase et

al., 2019; Igberase & Osifo, 2015, 2019b). Therefore, breakthrough curves were used to study the adsorption rate. Pb(II) concentration in the effluent was calculated as a function of time after a Pb(II) solution was allowed to pass through the membrane. Innovative tests were conducted using various transmembrane pressures, membrane thicknesses, and Lead concentrations.

**Column kinetics.** The kinetic equations applied by (Osifo et al., 2017) was also used in modelling the column data. According to the current model, the adsorbate is predicted to be bound in the active core, which as the binding process progresses vigorously enters the interior of the adsorbent. Additionally, the main mass transfer resistance for the binding process is intraparticle diffusion through the adsorbate-filled shell, which follows the distribution equation shown in Eq. [8]:

$$\frac{\partial q}{\partial t} = \frac{k_L a \frac{3D_{eff}}{R_s^2 \rho \left( \frac{1 - (1 - \theta)^{1/3}}{(1 - \theta)^{1/3}} \right)}}{k_L a + \frac{3D_{eff}}{R_s^2 \rho \left( \frac{1 - (1 - \theta)^{1/3}}{(1 - \theta)^{1/3}} \right)}} C_B \quad [8]$$

where:  $D_{eff}$  is the effective diffusion coefficient (m<sup>2</sup>/s),  $C_B$  is the bulk mixture's adsorbate concentration (mmol/L),  $R$  is the bead's radius (m),  $\rho$  is the adsorbent's density (kg/m<sup>3</sup>), and is the fraction loading capacity.

$$\theta = q(t)/q_e \quad [9]$$

From the start of binding until equilibrium is reached, the ratio of the metal loading to the overall capacity changes. The effective diffusion coefficient can be fitted using Eq. 10, based on equilibrium values acquired from the experiment's calculation of the time-dependent binding and determined value of  $q_e$ . Figure 9 shows the experimental breakthrough curves for Pb(II) feed solutions with Pb(II) concentration at 7.65 mmol.L<sup>-1</sup> with an applied transmembrane pressure differential of 100 kPa and a pH of 5. The dimensionless concentration ( $C_t/C_{in}$ ) is shown in this figure as a function of how many.

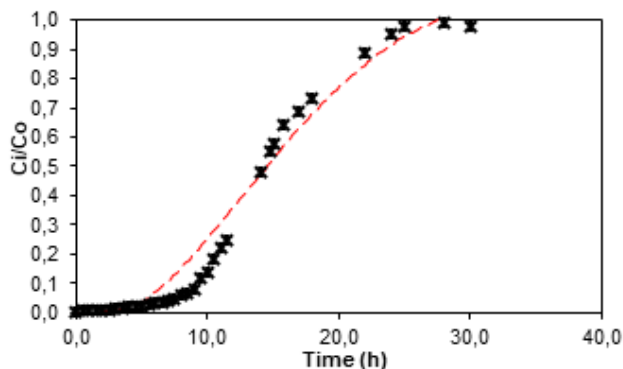


**Figure 9.** The breakthrough profile of Pb(II) solutions (pH = 5, and temperature at 298K).

equivalent membrane volumes are permitted to pass through the membrane. Pb(II) input and permeate concentrations are  $C_{in}$  and  $C_t$ , respectively.

The number of equivalent membrane volumes can be calculated from Figure 9 as the breakthrough if the breakthrough is defined at a concentration of 10% of the inlet concentration ( $C_t/C_{in} = 0.1$ ), at

which point the concentration of Pb(II) in the permeate reaches 10% of the Pb(II) concentration in the feed. These values are shown in Table 3 as the breakthrough. Since chitosan membranes have a modest equivalent membrane volume for feed solutions containing  $7.65 \text{ mmol.L}^{-1}$  Pb(II), it is likely that these applications will not require very high metal ion concentrations.

It was determined from a mass balance that breakthrough happened at 2% of the membrane's capacity, regardless of the solute concentration.

Even though chitosan has a higher adsorption capacity towards Cu(II) than Pb(II), the bed volume where breakthrough occurs for Cu(II) using chitosan beads is clearly smaller than that of Pb(II) using a chitosan membrane (II). Thus, it may be said that chitosan membranes can handle a larger equivalent membrane volume than beads. This behaviour is once more explained by the increased contact between the water and the adsorbent brought on by convective transport.

Parameters	value
Solution pH	5.0
N and m	1.0
Mass of beads (g)	120
Density ( $\text{kg/m}^3$ )	1100
Equilibrium constant ( $K_{ads}$ )	0.00119
Capacity of adsorbent ( $\text{mmol/g}$ )	4.1
Specific surface area ( $a$ ) ( $\text{m}^2/\text{kg}$ )	70.3
External mass transfer coefficient ( $k$ ) ( $\text{m/s}$ )	$5.2 \times 10^{-6}$
Lead diffusion coefficient in water ( $D_{Lead}$ ) ( $\text{m}^2/\text{s}$ )	$7.4 \times 10^{-9}$

**Table 3:**

*Variables applied in predicting experimental data.*

### The effect of cations and anions on membrane adsorption

A reference solution containing  $5.55 \text{ mmol.L}^{-1}$  lead was used to examine the impact of additional pollutants on the chitosan adsorption. Nine samples of the reference solution were taken, and these samples were then separated into three groups of samples. The reference solution was used as the benchmark for all pollutants. The effects of nitrates and chlorides on the adsorption capacity were assessed using the first set of samples; the effects of calcium, sodium, potassium, and magnesium were tested using the second set of samples; and the ef-

fects of sulphates were assessed using the third set of samples by increasing the concentration of sulphate in the sample. Using a 0.8 mm membrane, the solutions were processed at 298 K and 100 kPa transmembrane pressure. As seen in Table 4, nitrates and, to a lesser extent, chlorides have a detrimental effect on the adsorption capacity, contrary to what Becker et al. claimed (Becker et al. 2000). Since it has been shown that nitrates do adsorb on chitosan in the pH range of 3 to 5, and to a lesser extent at pH 6, competitive adsorption may occur in the case of nitrates (Jaafari et al., 2004b). (Kurita et al., 2003a) similarly documented a decrease in adsorption capacity caused by chlorides, and they attributed this

to the creation of different lead-chloro complexes. Normal rinse water has low nitrate concentrations but high chloride concentrations, which may hinder the adsorption of chitosan membranes. In light of the influence of chlorides on adsorption capacity, sodium, potassium, magnesium, and calcium do not significantly alter adsorption capacity and do not prohibit the simultaneous adsorption of lead metal ions. (El-Hefnawy et al., 2014) also noted this and

discovered that the presence of calcium and magnesium ions had no effect on the adsorption of cadmium ions. Nevertheless, a marginal rise in adsorption capacity with sulphate content was observed. This result can be attributed to chitosan's sulfate-induced structural changes, and (Mitani et al., 1991) have also noted an increased ability for transition metal ion adsorption in sulfate media.

**Table 4.** *The effect of cations and anions on membrane adsorption.*

Set	Pollutant	Concentration (mmol.L <sup>-1</sup> )								q/q <sub>ref</sub>
		Pb	SO <sub>4</sub>	NO <sub>3</sub>	Cl	K	Mg	Na	Ca	
Ref.	PbSO <sub>4</sub>	5.55	5.55	-	-	-	-	-	-	100%
	PbSO <sub>4</sub>	0.34	0.34	-	-	-	-	-	-	100%
1	Pb(NO <sub>3</sub> ) <sub>2</sub>	0.34	-	1.61	-	-	-	-	-	79%
	PbCl <sub>2</sub>	0.34	-	-	1.51	-	-	-	-	88%
2	KCl	-	-	-	1.39	1.53	-	-	-	85%
	MgCl <sub>2</sub> .2H <sub>2</sub> O	-	-	-	1.41	-	0.82	-	-	86%
	NaCl	-	-	-	1.41	-	-	1.40	-	89%
	CaCl <sub>2</sub> .2H <sub>2</sub> O	-	-	-	1.41	-	-	-	0.80	95%
3	CaCl <sub>2</sub> .2H <sub>2</sub> O	-	-	-	2.88	-	-	-	1.32	88%
	CaSO <sub>4</sub> .2H <sub>2</sub> O	-	1.31	-	-	-	-	-	1.32	89%

### Desorption and recovery

Adsorption was performed first on the membranes that had been prepared for desorption studies. Each membrane was exposed to a 7.65 mmol.L<sup>-1</sup> Pb(II) solution with a pH of 6 during the adsorption process. To ascertain the equilibrium adsorption capacity, the concentration of the Pb(II) solution both before and after treatment was analysed. Desorption, or recovery, was accomplished by treating the membranes with distilled water, solutions of hydrochloric acid (pH = 3 and 5), and solutions of sulphuric acid (pH = 3 and 5), in separate tests. The membranes were submerged in an acidic solution for six hours. Each treatment utilized 200 mL of acid and water, respectively.

Table 5 summarizes the percentage membrane mass loss during the regeneration treatment as well as the percentage of Pb(II) that was desorbed (calculated on the amount that was adsorbed). It was discovered that water did not desorb any appreciable quantities of Pb(II)-ions..

However, it was shown that sulphuric acid provided a higher percentage recovery (95%) than hydrochloric acid (89%).

The membrane loss throughout the recovery process while using hydrochloric acid (up to 7%) was greater than when using sulphuric acid (up to 5%). Sulphuric acid is therefore determined to be a superior regeneration agent to hydrochloric acid. Furthermore, Chitosan has been demonstrated to be less soluble in sulphuric acid than in hydrochloric, nitric, or organic acids by (Milot et al., 1998). So, sulphuric acid was employed to explore how many cycles a membrane may withstand before degrading and losing its mechanical strength.

The most effective desorption agent (H<sub>2</sub>SO<sub>4</sub>, pH=3) was used in multi-cycle trials. With a percentage recovery of 70% (based on the new adsorption capacity) and a mass loss of 11% after the second cycle, the adsorption capacity was lowered to 75% of the initial adsorption capacity (based on the ori-

Eluent	pH	% Desorption	Weight loss (%)
Water	7.1	3%	0%
HCl	3	89%	7%
HCl	5	68%	4%
H <sub>2</sub> SO <sub>4</sub>	3	95%	5%
H <sub>2</sub> SO <sub>4</sub>	5	73%	2%

**Table 5.** Desorption/adsorption process.

ginal membrane mass). It was discovered that the membrane can only be regenerate at most twice before losing a considerable amount of its structural integrity.

### Reaction mechanism of chitosan

Various interactions, including chelation, electrostatic, hydrophobic, electron donor, and polarity, can result in the adsorption of lead on chitosan (Li et al. 2012). Although the presence of hydrophilic groups like amine (-NH<sub>2</sub>) and hydroxyl (-OH) on the backbone of chitosan can make it polar, these reactive groups react with metal ions depending on factors like the type of metal, the pH, the fraction of deacetylated units (free amine groups), polymer chain length, crystallinity, molecular weight, conditioning of polymers, physical form of chitosan, solution pH, type and concentration of the acid (Igberase et al., 2017a).

Chitosan and lead metal can, however, be surrounded by water molecules due to their polar nature. For polar interaction to take place, the water molecules adsorbed on the adsorbate and adsorbent surfaces (via inter- or intramolecular hydrogen bonding) has to be disrupted and the adsorbate molecules replace the water molecules on the adsorbent surface (Mao et al., 2021). Solvent replacement is the term for this procedure.

From another angle, the coordinate connection between the metal ions and the amine group is started by the amine group. It is created by the free electron pairs of the nitrogen in the amine group and the empty orbitals of the metal. Additionally, at pH levels close to neutrality and at lower pH levels, where protonation of the amine group occurs, the free electron doublet of nitrogen on amine groups is responsible for the adsorption of metal cations; the polymer then develops cationic groups that can electrostatically bind anions. (Igberase et al., 2017a).

### Conclusions

According to equilibrium isotherm investigations, a maximum Pb(II) adsorption capacity of 2.98 mmol.g<sup>-1</sup> of chitosan for temperatures between 303 and 313 K can be used to explain the adsorption of Pb(II) by XCSM. Additionally, an endothermic adsorption process with an adsorption enthalpy of 52 kJ.mol<sup>-1</sup> was discovered.

The initial concentration of Pb(II) in the solution had an impact on Pb(II) breakthrough, although it was discovered that chitosan membranes outperformed other chitosan topologies, such as beads. This is because dense chitosan membranes have a higher adsorption capacity than beads, leading to more efficient interaction between the adsorbate and chitosan adsorbent when utilized as a dense adsorption layer, or membrane. As the membrane flux was increased from 1.36-1.96 L.m<sup>-2</sup>.hr<sup>-1</sup>, it was demonstrated that the adsorption process is also kinetically controlled.

Additionally, it was demonstrated that co-ions and the solution's pH have an impact on the adsorption of metal ions by XCSM. Nitrates inhibit the adsorption, and sulphates promote it. The ideal pH for Pb(II) adsorption by chitosan membranes was discovered to be at a pH lower than 6.

The high metal-ion concentration that comes from the adsorption of metal ions from solution using this membrane arrangement can be recovered by washing the chitosan membranes with an acidic solution. Pb(II) was removed with an efficiency of 95% as the pH of the recovery solution was lowered from pH 6 to pH 3, all the while regenerating the chitosan membranes. However, regeneration reduced the adsorption capacity of the chitosan membranes, mostly as a result of up to 11% mass loss of the membrane. The membrane's structural integrity was compromised after two regeneration cycles, making it impossible to use the membrane again.

## References

- AYUB A., RAZA ZA. (2021) Arsenic removal approaches: A focus on chitosan biosorption to conserve the water sources. *International Journal of Biological Macromolecules*, 192:1196–1216. <https://doi.org/10.1016/j.ijbiomac.2021.10.050>
- BARIQUE M.A., TSUCHIDA E., OHIRA A., TASHIRO K. (2017) Effect of Elevated Temperatures on the States of Water and Their Correlation with the Proton Conductivity of Nafion. *ACS Omega*, 3:349–360. <https://doi.org/10.1021/acsomega.7b01765>
- BASSI R., PRASHER S.O., SIMPSON B.K. (2000) Removal of selected metal ions from aqueous solutions using chitosan flakes. *Separation Science and Technology*, 35:547–560. <https://doi.org/10.1081/SS-100100175>
- BECKER T., SCHLAAK M., STRASDEIT H. (2000) Adsorption of nickel(II), zinc(II) and cadmium(II) by new chitosan derivatives. *Reactive and Functional Polymers*, 44:289–298. [https://doi.org/10.1016/S1381-5148\(99\)00104-2](https://doi.org/10.1016/S1381-5148(99)00104-2)
- BOUHAMED F., ELOUEAR Z., BOUZID J. (2012) Adsorptive removal of copper(II) from aqueous solutions on activated carbon prepared from Tunisian date stones: Equilibrium, kinetics and thermodynamics. *Journal of Taiwan Institute of Chemical Engineering*, 43:741–749. <https://doi.org/10.1016/j.jtice.2012.02.011>
- CERVERA M.L., ARNAL M.C., DELA GUARDIA M. (2003) Removal of heavy metals by using adsorption on alumina or chitosan. *Analytical and Bioanalytical Chemistry*, 375:820–825. <https://doi.org/10.1007/s00216-003-1796-2>
- CHUI V., MOK K., NG C. (1996) Removal and recovery of copper (II), chromium (III), and nickel (II) from solutions using crude shrimp chitin packed in small columns. *Environment International*, 22:463–468. [https://doi.org/10.1016/0160-4120\(96\)00034-7](https://doi.org/10.1016/0160-4120(96)00034-7)
- EL-HEFNAWY M.E., SELIM E.M., ASSAAD F.F., ISMAIL A.I. (2014) The effect of chloride and sulfate ions on the adsorption of Cd<sup>2+</sup> on clay and sandy loam egyptian soils. *The Scientific World Journal*, 2014. <https://doi.org/10.1155/2014/806252>
- FAROOQ U., KOZINSKI J.A., KHAN M.A., ATHAR M. (2010) Biosorption of heavy metal ions using wheat based biosorbents - A review of the recent literature. *Bioresour Technol*, 101:5043–5053. <https://doi.org/10.1016/j.biortech.2010.02.030>
- FINSTER M.E., RAYMOND M.R., SCOFIELD M.A., SMITH KP. (2015) Mercury-impacted scrap metal: Source and nature of the mercury. *Journal of Environmental Management*, 161:303–308. <https://doi.org/10.1016/j.jenvman.2015.05.041>
- GE H., HUA T. (2016) Synthesis and characterization of poly(maleic acid)-grafted crosslinked chitosan nanomaterial with high uptake and selectivity for Hg(II) sorption. *Carbohydrate Polymers* 153:446–452. <https://doi.org/10.1016/j.carbpol.2016.07.110>
- GE H., HUA T., CHEN X. (2016) Selective adsorption of lead on grafted and crosslinked chitosan nanoparticles prepared by using Pb<sup>2+</sup> as template. *Journal of Hazardous Material* 308:225–232. <https://doi.org/10.1016/j.jhazmat.2016.01.042>
- GENG J., LIN L., GU F., CHANG J. (2022) Adsorption of Cr(VI) and dyes by plant leaves: Effect of extraction by ethanol, relationship with element contents and adsorption mechanism. *Industrial Crops and Products* 177. <https://doi.org/10.1016/J.INDCROP.2022.114522>
- GUIBAL E. (2004) Interactions of metal ions with chitosan-based sorbents: A review. *Separation and Purification Technology*, 38:43–74. <https://doi.org/10.1016/j.seppur.2003.10.004>
- HO YS., MCKAY G. (2002) Application of Kinetic Models to the Sorption of Copper (II) on to Peat. *Adsorption Science & Technology*, 20:797–815. <https://doi.org/10.1260/026361702321104282>
- IGBERASE E., OSIFO P., OFOMAJA A. (2014) The adsorption of copper (II) ions by polyaniline graft chitosan beads from aqueous solution: Equilibrium, kinetic and desorption studies. *Journal of Environmental Chemical Engineering* 2:362–369. <https://doi.org/10.1016/j.jece.2014.01.008>
- IGBERASE E., OSIFO P. (2015) Equilibrium, kinetic, thermodynamic and desorption studies of cadmium and lead by polyaniline grafted cross-linked chitosan beads from aqueous solution. *Journal of Industrial and Engineering Chemistry*, 26:340-347. <https://doi.org/10.1016/j.jiec.2014.12.007>
- IGBERASE E., OSIFO P., OFOMAJA A. (2017A) The Adsorption of Pb, Zn, Cu, Ni, and Cd by Modified Ligand in a Single Component Aqueous Solution: Equilibrium, Kinetic, Thermodynamic, and Desorption Studies. *International Journal of Analytical Chemistry* 2017:1-15. <https://doi.org/10.1155/2017/6150209>
- IGBERASE E., OSIFO P., OFOMAJA A. (2017B) Mathematical modelling of Pb<sup>2+</sup>, Cu<sup>2+</sup>, Ni<sup>2+</sup>, Zn<sup>2+</sup>, Cr<sup>6+</sup> and Cd<sup>2+</sup> ions adsorption from a synthetic acid mine drainage onto chitosan derivative in a packed bed column. *Environmental Technology*, (United Kingdom). <https://doi.org/10.1080/09593330.2017.1375027>
- IGBERASE E., OFOMAJA A., OSIFO P.O. (2019) Enhanced heavy metal ions adsorption by 4-aminobenzoic

- acid grafted on chitosan epichlorohydrin composite: Kinetics, isotherms, thermodynamics and desorption studies. *International Journal of Biological Macromolecules*, 123:. <https://doi.org/10.1016/j.ijbiomac.2018.11.082>
- IGBERASE E, OSIFO PO (2019A) Application of diethylenetriamine grafted on glyoxal cross-linked chitosan composite for the effective removal of metal ions in batch system. *International Journal of Biological Macromolecules*, 134:1145–1155. <https://doi.org/10.1016/j.ijbiomac.2019.05.179>
- IGBERASE E., OSIFO P.O. (2019B) Mathematical modelling and simulation of packed bed column for the efficient adsorption of Cu(II) ions using modified biopolymeric material. *Journal of Environmental Chemical Engineering* 7:103-129. <https://doi.org/10.1016/j.jece.2019.103129>
- JAAFARI K., RUIZ T., ELMALEH S. (2004) Simulation of a fixed bed adsorber packed with protonated cross-linked chitosan gel beads to remove nitrate from contaminated water. *Chemical Engineering Journal* 99:153–160. <https://doi.org/10.1016/j.ccej.2003.10.008>
- JIN C., LIU G., WU G. (2020) Facile fabrication of crown ether functionalized lignin-based biosorbent for the selective removal of Pb(II). *Industrial Crops and Products*, 155.. <https://doi.org/10.1016/j.indcrop.2020.112829>
- KURITA K., AKAO H., YANG J., SHIMOJOH M. (2003A) Nonnatural branched polysaccharides: Synthesis and properties of chitin and chitosan having disaccharide maltose branches. *Biomacromolecules*, 4:1264–1268. <https://doi.org/10.1021/bm034074p>
- LIMA I.S., AIROLDI C. (2004) A thermodynamic investigation on chitosan-divalent cation interactions. *Thermochimica Acta* 421:133–139. <https://doi.org/10.1016/j.tca.2004.03.012>
- MADHAVA RAO M, RAMESH A, PURNA CHANDRA RAO G, SESHIAIAH K (2006) Removal of copper and cadmium from the aqueous solutions by activated carbon derived from Ceiba pentandra hulls. *Journal of Hazardous Materials*, 129:123–129. <https://doi.org/10.1016/j.jhazmat.2005.08.018>
- MAO M., YAN T., SHEN J. (2021) Capacitive removal of heavy metal ions from wastewater via an electro-Adsorption and electro-reaction coupling process. *Environmental Science and Technology*, 55:3333–3340. <https://doi.org/10.1021/ACS.EST.0C07849>
- MILOT C., MCBRIEN J., ALLEN S., GUIBAL E. (1998) Influence of physicochemical and structural characteristics of chitosan flakes on molybdate sorption. *Journal of Applied Polymer Science*, 68:571–580. [https://doi.org/10.1002/\(SICI\)1097-4628\(19980425\)68:4<571::AID-APP8>3.3.CO;2-1](https://doi.org/10.1002/(SICI)1097-4628(19980425)68:4<571::AID-APP8>3.3.CO;2-1)
- MITANI T., FUKUMURO N., YOSHIMOTO C., ISHII H. (1991) Effects of counter ions (SO<sub>4</sub><sup>2-</sup> and Cl<sup>-</sup>) on the adsorption of copper and nickel ions by swollen chitosan beads. *Agricultural and Biological Chemistry*, 55:2419. <https://doi.org/10.1080/00021369.1991.10870942>
- MO Y., WANG S., VINCENT T. (2019) New highly-percolating alginate-PEI membranes for efficient recovery of chromium from aqueous solutions. *Carbohydrate Polymers*, 225:115-177. <https://doi.org/10.1016/j.carbpol.2019.115177>
- Mokhtar A., Abdelkrim S., Boukoussa B. (2023) Elimination of toxic azo dye using a calcium alginate beads impregnated with NiO/activated carbon: Preparation, characterization and RSM optimization. *International Journal of Biological Macromolecules* 233:123-582. <https://doi.org/10.1016/j.ijbiomac.2023.123582>
- NGAH W.S.W., ABGHANI S., KAMARI A. (2005) Adsorption behaviour of Fe(II) and Fe(III) ions in aqueous solution on chitosan and cross-linked chitosan beads. *Bioresource Technology*, 96:443–450. <https://doi.org/10.1016/j.biortech.2004.05.022>
- OMOROGIE M.O., BABALOLA J.O., UNUABONAH E.I. (2016) Efficient chromium abstraction from aqueous solution using a low-cost biosorbent: *Nauclea diderrichii* seed biomass waste. *Journal of Saudi Chemical Society*, 20:49–57. <https://doi.org/10.1016/j.jscs.2012.09.017>
- OSIFO P.O., NEOMAGUS H.W.J.P., VAN DER MERWE H., BRANKEN D.J. (2017) Transport properties of chitosan membranes for zinc (II) removal from aqueous systems. *Separation and Purification Technology*, 179:428–437. <https://doi.org/10.1016/j.seppur.2017.02.030>
- PAL P., PAL A. (2019) Treatment of real wastewater: Kinetic and thermodynamic aspects of cadmium adsorption onto surfactant-modified chitosan beads. *International Journal of Biological Macromolecules* 131:1092–1100. <https://doi.org/10.1016/j.ijbiomac.2019.03.121>
- QASEM N.A.A., MOHAMMED R.H., LAWAL D.U. (2021) Removal of heavy metal ions from wastewater: a comprehensive and critical review. *NPJ Clean Water* 4:. <https://doi.org/10.1038/S41545-021-00127-0>
- QU J., MENG Q., LIN X. (2021) Microwave-assisted synthesis of  $\beta$ -cyclodextrin functionalized celluloses for enhanced removal of Pb(II) from water: Adsorptive performance and mechanism exploration. *Science of the Total Environment*, 752:141-854. <https://doi.org/10.1016/j.scitotenv.2020.141854>
- RAO M.M., RAO G.P.C., SESHIAIAH K. (2008) Activated carbon from Ceiba pentandra hulls, an agricul-

tural waste, as an adsorbent in the removal of lead and zinc from aqueous solutions. *Waste Management*, 28:849–858. <https://doi.org/10.1016/j.wasman.2007.01.017>

ROJAS G., SILVA J., FLORES J.A. (2005) Adsorption of chromium onto cross-linked chitosan. *Separation and Purification Technology*, 44:31–36. <https://doi.org/10.1016/j.seppur.2004.11.013>

SAJJADI SA., MEKNATI A., LIMA E.C. (2019) A novel route for preparation of chemically activated carbon from pistachio wood for highly efficient Pb(II) sorption. *Journal of Environmental Management*, 236:34–44. <https://doi.org/10.1016/j.jenvman.2019.01.087>

SHETH Y., DHARASKAR S., KHALID M., SONAWANE S. (2021) An environment friendly approach for heavy metal removal from industrial wastewater using chitosan based biosorbent: A review. *Sustainable Energy Technologies and Assessments*, 43:100-951. <https://doi.org/10.1016/j.seta.2020.100951>

SINGH V.K., KUSHWAHA C.S., SHUKLA S.K. (2020) Potentiometric detection of copper ion using chitin graf-

ted polyaniline electrode. *International Journal of Biological Macromolecules*, 147:250–257. <https://doi.org/10.1016/j.ijbiomac.2019.12.209>

TATY-COSTODES V.C., FAUDET H., PORTE C., HO Y.S. (2005) Removal of lead (II) ions from synthetic and real effluents using immobilized *Pinus sylvestris* sawdust: Adsorption on a fixed-bed column. *Journal of Hazardous Materials*, 123:135–144. <https://doi.org/10.1016/j.jhazmat.2005.03.032>

WAN NGAH W.S., TEONG L.C., TOH R.H., HANAFIAH M. (2012) Utilization of chitosan-zeolite composite in the removal of Cu(II) from aqueous solution: Adsorption, desorption and fixed bed column studies. *Chemical Engineering Journal*, 209:46–53. <https://doi.org/10.1016/j.cej.2012.07.116>

YU W., HU J., YU Y. (2021) Facile preparation of sulfonated biochar for highly efficient removal of toxic Pb(II) and Cd(II) from wastewater. *Science of the Total Environment*, 750:141-545. <https://doi.org/10.1016/j.scitotenv.2020.141545>